Supplementary Information

Measurement report: Size distributions of urban aerosols down to 1 nm from long-term measurements

Chenjuan Deng[1], Yiran Li[1], Chao Yan[2,3,4], Jin Wu[1], Runlong Cai[2], Dongbin Wang[1], Yongchun Liu[3], Juha Kangasluoma[2,3,5], Veli-Matti Kerminen[2], Markku Kulmala[2,3,4], Jingkun Jiang[1,*]

[1]State Key Joint Laboratory of Environment Simulation and Pollution Control, School of Environment, Tsinghua University, 100084 Beijing

[2]Institute for Atmospheric and Earth System Research/Physics, Faculty of Science, University of Helsinki, 00014 Helsinki, Finland

[3]Aerosol and Haze Laboratory, Beijing Advanced Innovation Center for Soft Matter Science and Engineering, Beijing University of Chemical Technology, 100029 Beijing, China

[4]Joint International Research Laboratory of Atmospheric and Earth System Sciences, School of Atmospheric Sciences, Nanjing University, Nanjing, China

[5]Karsa Ltd., A. I. Virtasen aukio 1, 00560 Helsinki, Finland

1. The schematics of DEG SMPS and PSD

Figure S1 shows the schematics and pictures of DEG SMPS and PSD. DEG SMPS sampled aerosols through the window of the observation room with a core sampling method (a transport flow of ~6.4 LPM was used). The aerosols then entered the neutralizer for charging and the mini-cyDMA for classification. Those classified aerosols were sent into the modified DEG-UCPC and CPC to grow through condensation and detect optically. PSD sampled aerosols through the inlet from the roof of the observation room. A PM_{10} impactor before the PSD inlet was used to remove larger particles. A Nafion dryer (Perma Pure, MD-700-24F-3) was used before the PSD inlet to control the relative humidity to be below 40%. An aerosol flow of 5 LPM was sampled by APS. The flow rate of the aerosol flow entering the parallel SMPSs was 1.8 LPM. These two SMPSs share a UCPC to detect classified aerosols. Two three-way valves helped to select the SMPS that the sample flow enters.

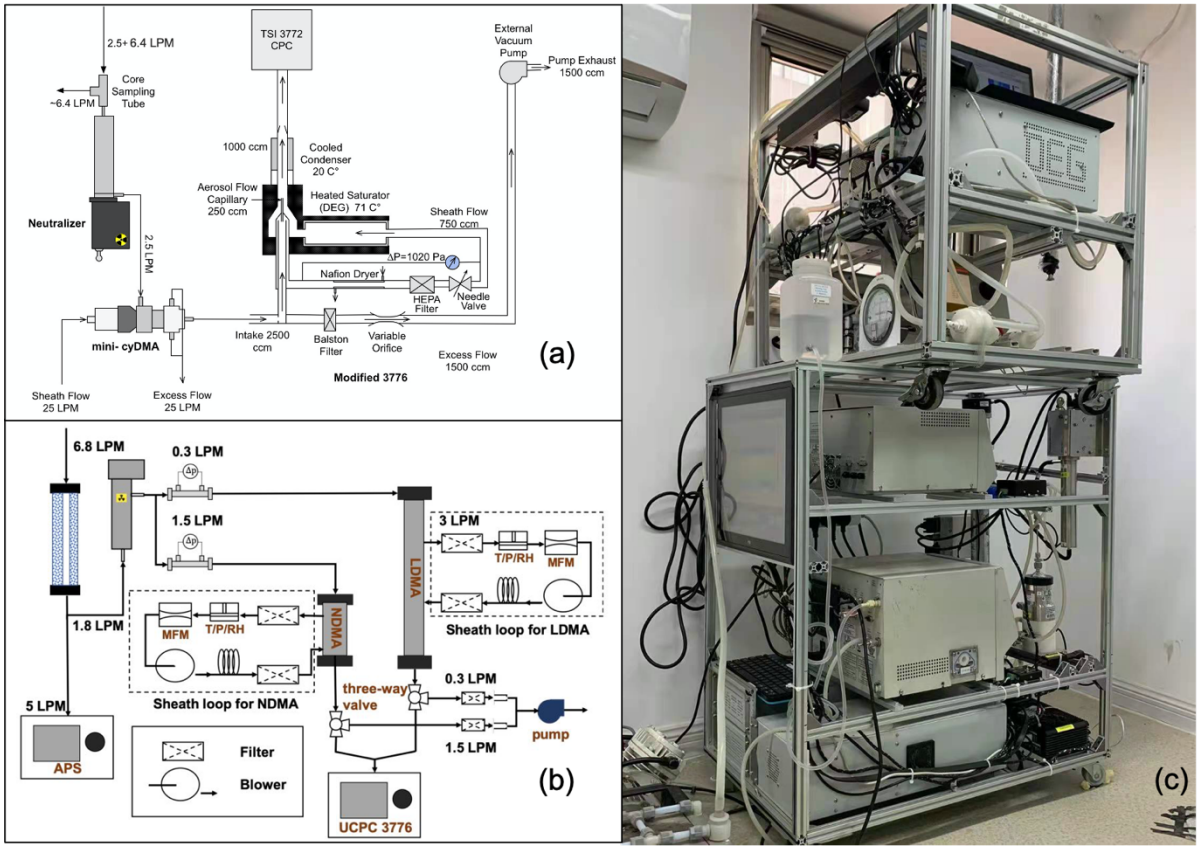

Figure S1. The schematics of (a) DEG SMPS and (b) PSD, and (c) their pictures.

2. Description of the cluster analysis

k-means clustering was used to identify typical types of atmospheric aerosol size distributions (Beddows et al., 2009; Wegner et al., 2012). We selected 4 indices to represent the characteristics of each set of 5-min measured aerosol number size distributions, including the diurnal variations of H_2SO_4 monomer and dimer concentration, diurnal variations of $N_{sub\text{-}3}$ and the contribution of $N_{sub\text{-}3}$ to the total number concentration. Each data point was normalized to the vector length by,

$$\frac{m_i}{\sqrt{\sum_{i=1}^{n}(m_i)^2}} \quad \text{(S1)}$$

where m_i can represent H_2SO_4 monomer and dimer concentration, and $N_{sub\text{-}3}$, cm^{-3}; when the index is the diurnal variations of H_2SO_4 monomer and dimer concentration, and $N_{sub\text{-}3}$, m_i represents H_2SO_4 monomer and dimer concentration, and $N_{sub\text{-}3}$ and they were divided by the Euclidean norm of the time series of m_i each day; when the index is the contribution of $N_{sub\text{-}3}$ to the total number concentration, m_i represents $N_{sub\text{-}3}$ and was divided by the Euclidean norm of particle number concentration in each time bin.

The *k*-means method divided the data into *k* clusters such that the "within-cluster sum of squares" (WSS) function is minimized using iteration. The degree of dissimilarity between two size distributions is defined as the distance. The distance function used in this study, which is also common-used elsewhere, is the Euclidean distance (Wilks, 2011).

As shown in Fig. S1, the WSS decreased dramatically as the number of clusters increased from 1 to 3. After this, the increase of number of clusters only decreases the WSS to a significantly less extent. Therefore, we chose 3 as the number of clusters.

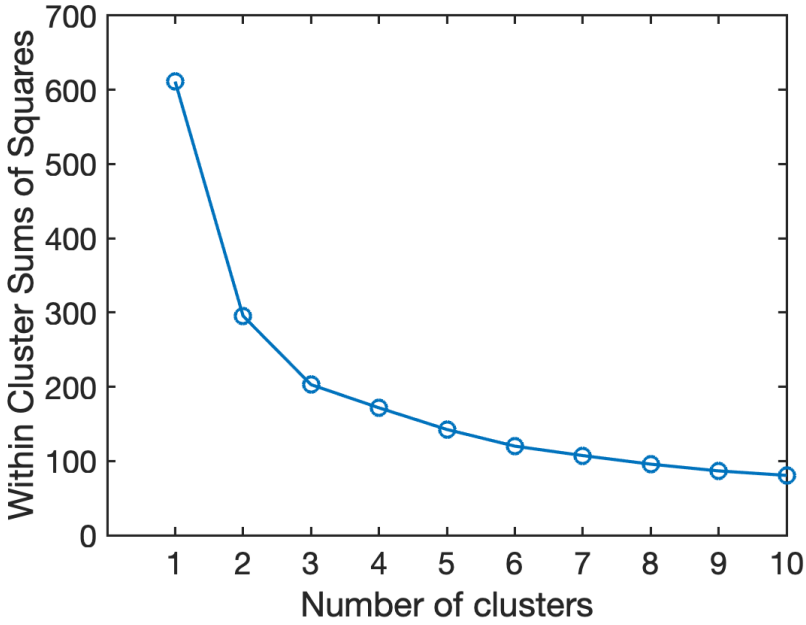

Figure S2. The relation between the number of clusters and the within cluster sums of squares (WSS).

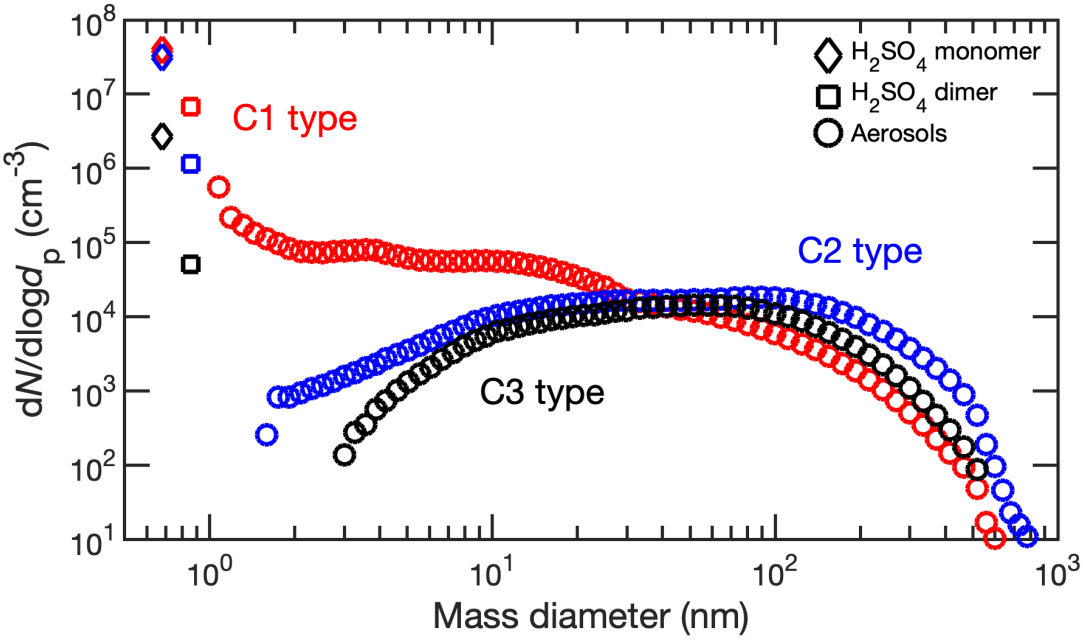

Figure S3. The median aerosol size distributions in three clusters. The diamonds, squares, and circles represent the distribution function (dN/dlogd_p) of H_2SO_4 monomers, dimers and aerosols, respectively.

3. Calculation of the indicator *I*

The indicator I can be calculated as,

$$I = \frac{\beta^3 [A_{1,tot}]^4}{CS^2} \eta^4 \quad \text{(S2)}$$

where $[A_{1,tot}]$ is the total number concentration of H_2SO_4 monomers measured by CIMS, cm^3; β represents the collision coefficient between two $(H_2SO_4)_1(amine)_1$ clusters, $cm^3 \cdot s^{-1}$; CS is the condensation sink, s^{-1}; the enhancement factor, 2.3 for β and 1.3 for CS, was used to account for the enhancement of van der Waals forces on the of coagulation between clusters; η represents the ratio of the $(H_2SO_4)_1(amine)_1$ cluster concentration to the total H_2SO_4 monomer concentration estimated by

$$\eta = \frac{[A_1B_1]}{[A_1] + [A_1B_1]} \approx \frac{\beta[B]}{\gamma(T) + CS + \beta[B]} \quad \text{(S3)}$$

where $[A_1B_1]$ indicates $(H_2SO_4)_1(amine)_1$ concentration, cm^3; $[A_1]$ represents the concentration of H_2SO_4 molecules, cm^3; γ represents the evaporation rate of $(H_2SO_4)_1(amine)_1$ as a function of ambient temperature T, s^{-1}; [B] is the amine concentration, cm^3. The median of measured amine concentration, 2.7 ppt, was used to calculate I (Cai et al., 2021).

The condensation sink (CS) characterizes the sink for condensing vapor caused by background aerosols. It was calculated using the method reported by Kulmala et al. (2001),

$$CS = 2\pi D \sum_{d_p} \beta_{m,d_p} d_p N_{d_p} \quad \text{(S4)}$$

where D is the diffusion coefficient of H_2SO_4 monomer, $m^2 \cdot s^{-1}$; d_p is the particle geometric mean diameter for the size bin, m; N_{d_p} is the concentration of particles in the size bin, m^{-3}; β_m is the transition-regime correction factor (Fuchs and Sutugin, 1971),

$$\beta_m = \frac{1 + K_n}{1 + 1.677K_n + 1.333{K_n}^2} \quad \text{(S5)}$$

where K_n is the Knudsen number, $K_n = 2\lambda/d_p$.

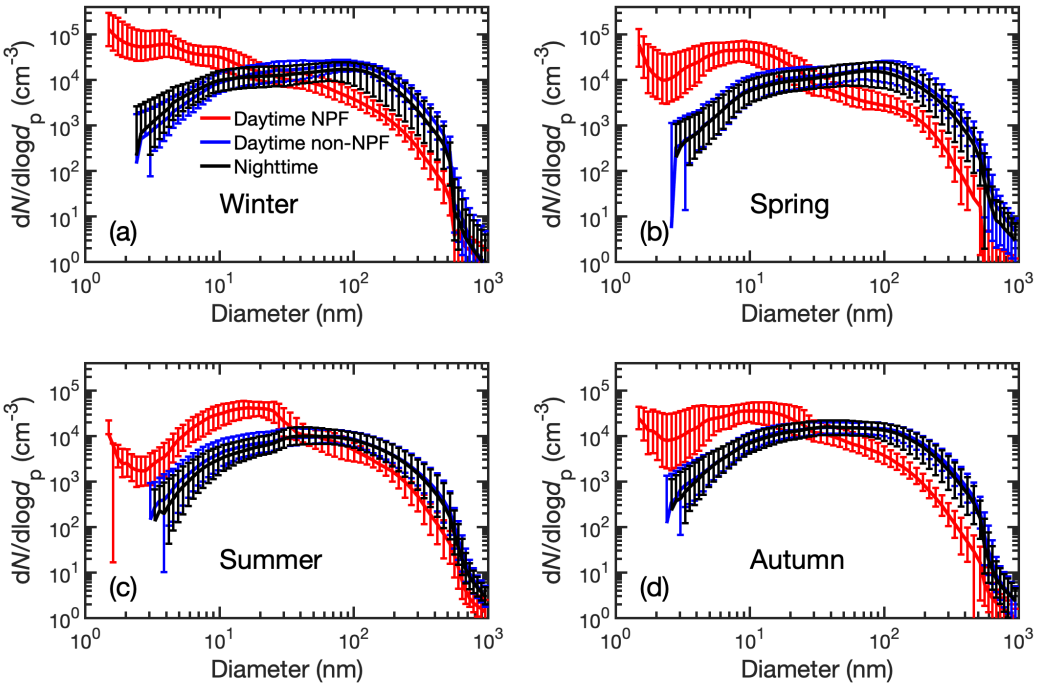

Figure S4. The median (solid lines), 25th percentiles (bottom edges of the error bars) and 75th percentiles (top edges of the error bars) aerosol size distributions of daytime NPF (red), daytime non-NPF (blue) and nighttime (black) type aerosol size distributions in (a) winter, (b) spring, (c) summer and (d) autumn.

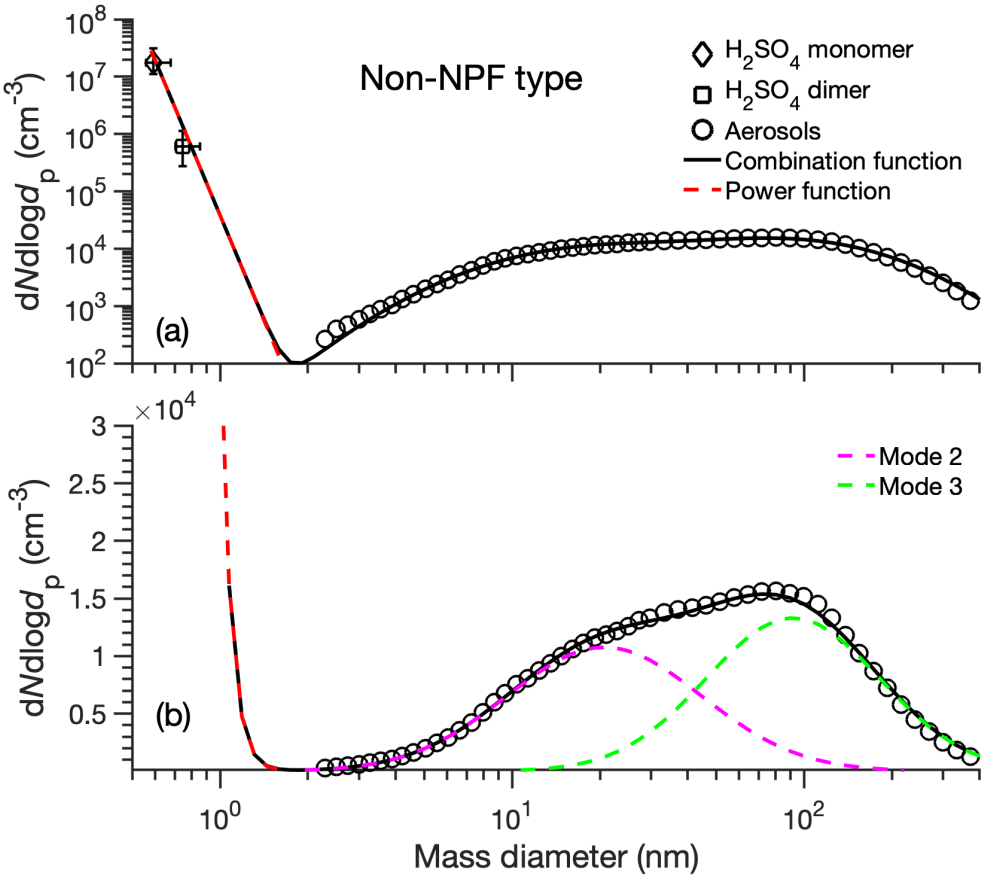

Figure S5. The median daytime non-NPF type number size distributions from H_2SO_4 monomer to larger particles and the fitted size distributions shown in (a) logarithm scale and (b) linear scale of y axis. The x-axis error bars of H_2SO_4 monomers and dimers indicate the variation range of estimated H_2SO_4 monomers and dimers diameters by assuming the bulk density to be 1000~1800 kg m^3. The y-axis error bars of H_2SO_4 monomers and dimers indicate the 25^{th}~75^{th} range of concentrations. The black and red lines indicate the fitted size distribution in whole size range and in sub-3 nm size range, respectively. The blue, magenta and green lines present the fitted mode 2 and mode 3, respectively. The diamonds, squares, and circles represent the distribution function ($dN/dlogd_p$) of H_2SO_4 monomers, dimers and aerosols, respectively.

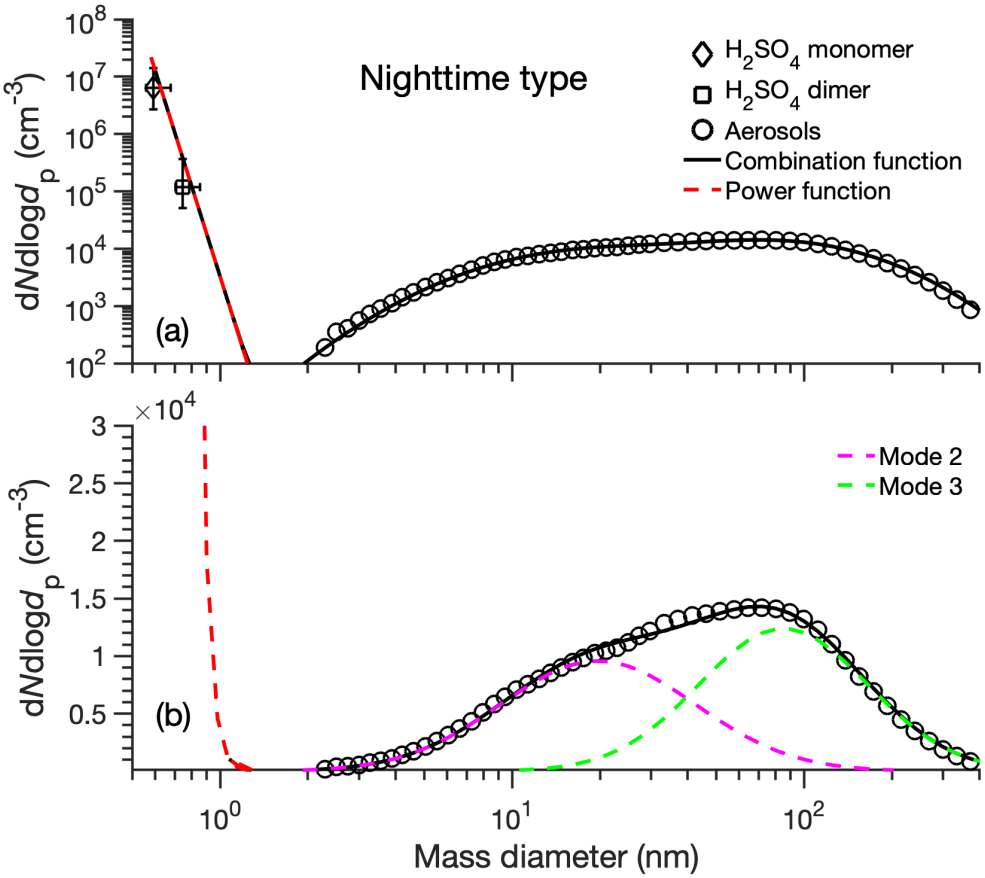

Figure S6. The median nighttime type number size distributions from H_2SO_4 monomer to larger aerosol size and the fitted size distributions shown in (a) logarithm scale and (b) linear scale of y axis. The x-axis error bars of H_2SO_4 monomers and dimers indicate the variation range of estimated H_2SO_4 monomers and dimers diameters by assuming the bulk density to be 1000~1800 kg m^3. The y-axis error bars of H_2SO_4 monomers and dimers indicate the 25^{th}~75^{th} range of concentrations. The black and red lines indicate the fitted size distribution in whole size range and in sub-3 nm size range, respectively. The blue, magenta and green lines present the fitted mode 2 and mode 3, respectively. The diamonds, squares, and circles represent the distribution function ($dN/d\log d_p$) of H_2SO_4 monomers, dimers and aerosols, respectively.

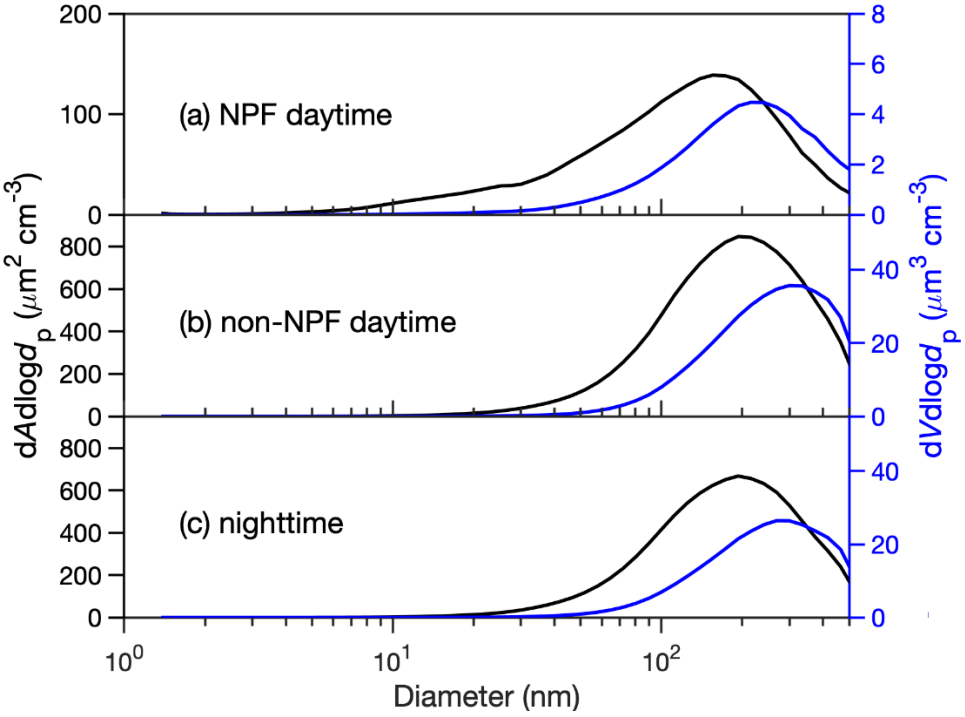

Figure S7. The surface area (dA/dlogd_p, black lines) and volume (dV/dlogd_p, blue lines) size distributions of the median NPF daytime, non-NPF daytime and nighttime types.

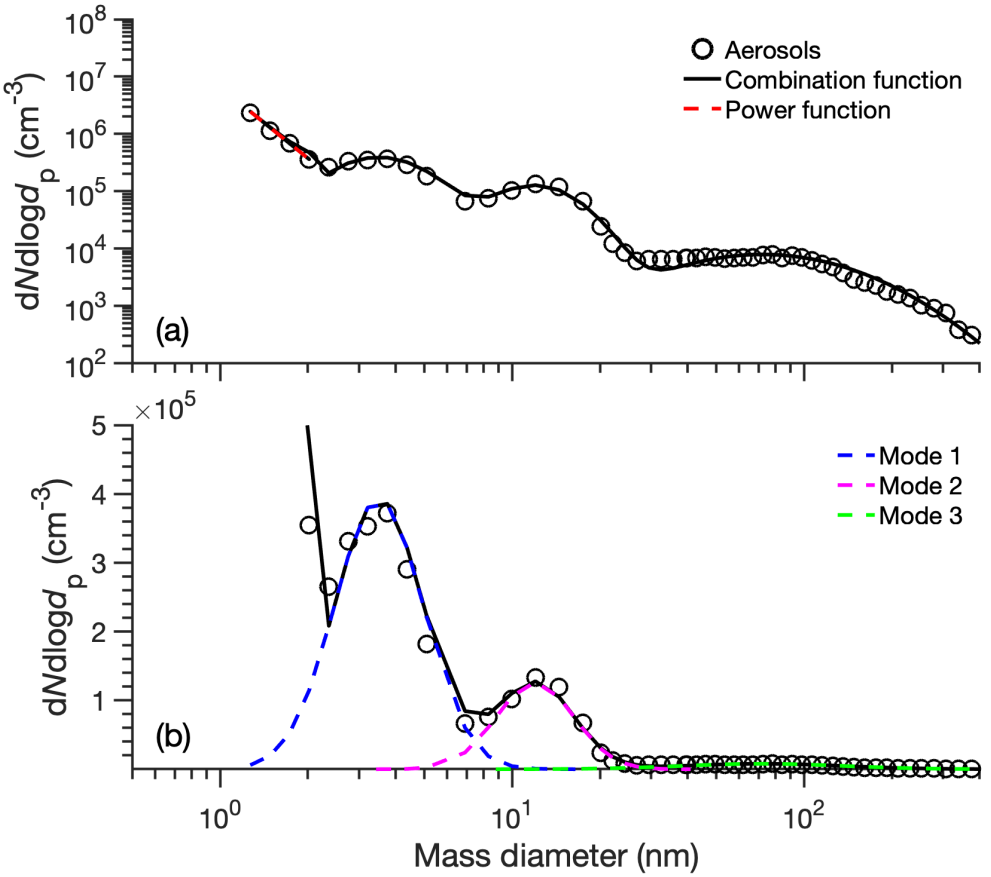

Figure S8. The median daytime NPF type aerosol number size distributions size and the fitted size distributions shown in (a) logarithm scale and (b) linear scale of y axis in Atlanta. The data was from the short-term campaign in Atlanta, Georgia, from July to August, 2009 (Jiang et al., 2011), which is the first study to measure the number size distributions of atmospheric sub-3 nm aerosols (Zhang et al., 2012). The black and red lines indicate the fitted size distribution in whole size range and in sub-3 nm size range, respectively. The blue, magenta and green lines present the fitted mode 1, mode 2 and accumulation mode, respectively. The circles represent the raw distribution function (dN/dlogd_p) of aerosols.

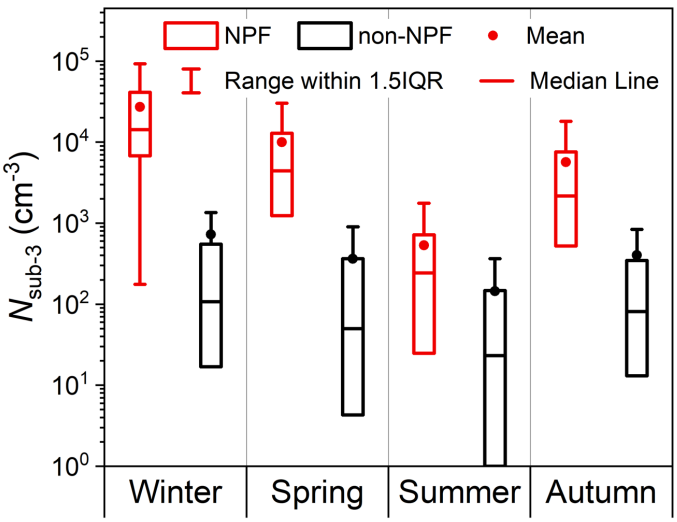

Figure S9. The seasonal variations of number concentrations of sub-3 nm aerosols (N_{sub-3}) on NPF days and non-NPF days during the measurement period. Data during 9:00 – 14:00 were used in this figure. The vertical lines and circles in the box indicate the median and mean values, respectively. The top and bottom edges represent 75th and 25th percentiles, respectively. The IQR is the interquartile range.

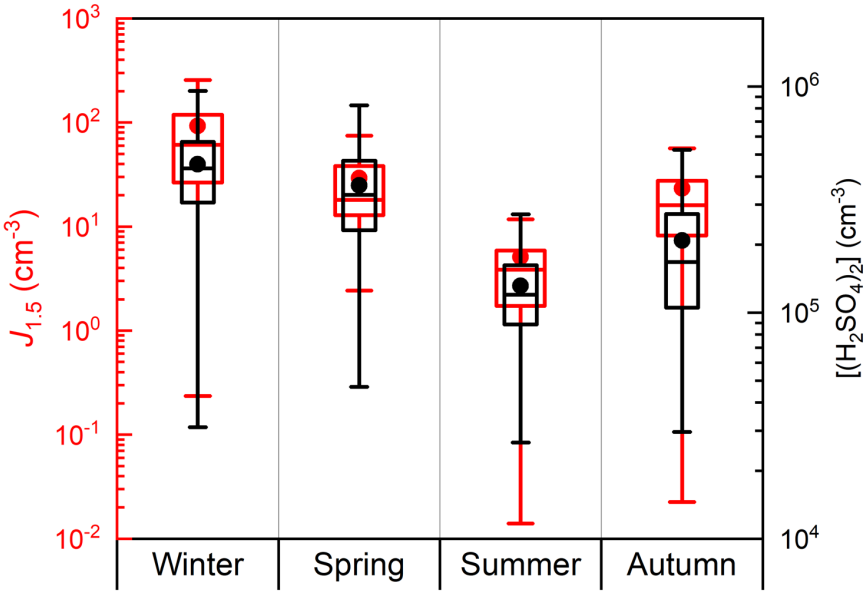

Figure S10. The seasonal variations of the formation rate of ~1.5 nm aerosols ($J_{1.5}$) and H_2SO_4 dimer concentration on NPF days during the measurement period. Data points during 9:00 – 14:00 were used in this figure. The vertical lines and circles in the box indicate the median and mean values, respectively. The top and bottom edges represent 75th and 25th percentiles, respectively.

References:

Beddows, D. C. S., Dall'Osto, M., and Harrison, R. M.: Cluster Analysis of Rural, Urban, and Curbside Atmospheric Particle Size Data, Environmental Science & Technology, 43, 4694-4700, https://doi.org/10.1021/es803121t, 2009.
Cai, R., Yan, C., Yang, D., Yin, R., Lu, Y., Deng, C., Fu, Y., Ruan, J., Li, X., Kontkanen, J., Zhang, Q., Kangasluoma, J., Ma, Y., Hao, J., Worsnop, D. R., Bianchi, F., Paasonen, P., Kerminen, V.-M., Liu, Y., Wang, L., Zheng, J., Kulmala, M., and Jiang, J.: Sulfuric acid–amine nucleation in urban Beijing, Atmospheric Chemistry and Physics, 21, 2457-2468, https://doi.org/10.5194/acp-21-2457-2021, 2021.
Fuchs, N. A., and Sutugin, A. G.: HIGH-DISPERSED AEROSOLS, in: Topics in Current Aerosol Research, edited by: Hidy, G. M., and Brock, J. R., Pergamon, 1, 1971.
Jiang, J., Zhao, J., Chen, M., Eisele, F. L., Scheckman, J., Williams, B. J., Kuang, C., and McMurry, P. H.: First Measurements of Neutral Atmospheric Cluster and 1–2 nm Particle Number Size Distributions During Nucleation Events, Aerosol Science and Technology, 45, ii-v, https://doi.org/10.1080/02786826.2010.546817, 2011.

Kulmala, M., Dal Maso, M., Mäkelä, J. M., Pirjola, L., Väkevä, M., Aalto, P., Miikkulainen, P., Hämeri, K., and O'dowd, C. D.: On the formation, growth and composition of nucleation mode particles, Tellus, 53, 479-490, 2001.
Wegner, T., Hussein, T., Hämeri, K., Vesala, T., Kulmala, M., and Weber, S.: Properties of aerosol signature size distributions in the urban environment as derived by cluster analysis, Atmospheric Environment, 61, 350-360, https://doi.org/10.1016/j.atmosenv.2012.07.048, 2012.
Wilks, D. S.: Statistical methods in the atmospheric sciences, Academic press, 2011.
Zhang, R., Khalizov, A., Wang, L., Hu, M., and Xu, W.: Nucleation and growth of nanoparticles in the atmosphere, Chem Rev, 112, 1957-2011, https://doi.org/10.1021/cr2001756, 2012.